A DFT/TDDFT Study of Porphyrazines and Phthalocyanine Oxo-Titanium Derivatives as Potential Dyes in Solar Cells

ARTICLE *in* INTERNATIONAL JOURNAL OF QUANTUM CHEMISTRY · DECEMBER 2011

Impact Factor: 1.43 · DOI: 10.1002/qua.22998

3 AUTHORS:

Ximena Zarate
Universidad Autónoma De Chile
32 PUBLICATIONS **90** CITATIONS
SEE PROFILE

Eduardo Schott
Pontifical Catholic University of Chile
50 PUBLICATIONS **294** CITATIONS
SEE PROFILE

Ramiro Arratia-Perez
Universidad Andrés Bello
149 PUBLICATIONS **1,201** CITATIONS
SEE PROFILE

A DFT/TDDFT Study of Porphyrazines and Phthalocyanine Oxo-Titanium Derivatives as Potential Dyes in Solar Cells

XIMENA ZARATE, EDUARDO SCHOTT, RAMIRO ARRATIA-PÉREZ

Departamento de Ciencias Químicas, Relativistic Molecular Physics Group, Universidad Andres Bello, República 275, Santiago, Chile

Received 27 October 2010; accepted 1 November 2010
Published online 1 February 2011 in Wiley Online Library (wileyonlinelibrary.com).
DOI 10.1002/qua.22998

ABSTRACT: Density functional theory and time dependent density functional theory calculations at the level of LDA/BP86/TZ2P were performed systematically on several Ti(IV) complexes of porphyrazines and one phthalocyanine. We performed an analysis of the frontier molecular orbitals of the ground state electronic structures and also discuss in particular the good concordance of our results with the experimental data, which affords to predict the geometrical and optical properties of new complexes (**3**, **4**, and **7**). We also emphasize the characterization of the UV–vis absorption spectra and propose transitions that contribute to the *Q* and *B* bands. Some useful calculated properties in complexes **2**, **3**, and **7**, like: high light absorption in the visible region of the spectra, transitions involved in these bands with a determined direction, charge separation, bigger highest occupied molecular orbital–lowest unoccupied molecular orbital (HOMO-LUMO) gaps than complexes **4** and **5**, and the energy of their LUMO orbitals (that are higher than the lowest energy level of the conduction band of the TiO_2) indicate that system complexes **2**, **3**, and **7** could act as light-harvesting sensitizers for dye-sensitized solar cells (DSCs). These proposals were made using a model of the previously experimentally known phthalocyanine, which was used as sensitizer in DSCs devices, comparing its electronic properties with the herein proposed sensitizers. Int J Quantum Chem 111: 4186–4196, 2011

Key words: DFT; TDDFT; porphyrazine; phthalocyanine; spectra

Correspondence to: R. Arratia-Pérez; e-mail: rarratia@unab.cl
Contract grant sponsor: Projects Millennium.
Contract grant numbers: P07-006-F, UNAB DI-26-10/I, UNAB DI-23-10/I, CONICYT AT24100024, CONICYT (to X.Z. and E.S.).

1. Introduction

The family of stable π-aromatic molecules, such as porphyrins draws interest in coordination chemistry because they are good electron donors and/or acceptors as well as sensitizers; they also show interesting molecular properties useful for redox catalysis, photocatalysis, dyes, and for building optical devices [1–3]. Nowadays, these complexes are considered to be excellent chromophores, with application in the design of dye-sensitized solar cells (DSC) [4–6]. A good example is the family of complexes reported by Campbell et al. [5] who designed a TiO_2-based nanocrystalline solar cells using porphyrins. Palomares et al. [6] described a titanium phthalocyanine (Pc) with catechol-COOH as axial ligand demonstrating the electron injection into a TiO_2 nano-particles, thus obtaining an efficient photocurrent generation in DSC, avoiding aggregation when is anchored to a semiconductor film mainly due to the *tert*-butyl (*t*Bu) substituents in the ring. In these cells, the sensitizer has the fundamental role of being responsible for pumping electrons from a lower to a higher energy level, thus making possible the generation of an electric potential difference, which is used to produce electric work. Today, there is a search of finding a sensitizer that achieves effective absorption of sunlight in the red and near-infrared region of the spectra to convert these photons into electricity [7–10]. Grätzel [11] developed the DSC and, until now, ruthenium(II) bipyridyl complexes have proven to be the most efficient TiO_2 sensitizers, but it is pertinent to mention that ruthenium is a special metal and its sources are limited, so novel inorganic dyes are desirable for highly efficient DSC [12–16]. On the other hand, the metallic complexes with porphyrin have showed conversion efficiencies near to Ru-bipyridyl complexes [4]. The task is to functionalize metalloporphyrins to compete with the Ru-based DSC.

The large sensitizer family of porphyrins-like includes porphyrazines (Pz), which because of complex synthetic pathway have not been worked out much in comparison with porphyrins. But owing to efficient synthetic routes reported by Fitzgerald et al. [16] and Rodríguez-Morgade and Stuzhin [17], it has increased the study of their properties and applications [18–23]. Pz is constituted by four tetrapyrroles and nitrogens in position *meso*, and also they are called tetra-azaporphyrins. Experimental and theoretical studies show a variety of tetra-azaporphyrin complexes with metallic center like Ti, Ni, Zn, and rare-earths, forming diverse types of dimers, trimers, and oligomers [18–20]. Similarly, density functional theory (DFT) and time dependent DFT (TDDFT) methodologies have been used by Muñoz-Castro et al. [24] to study the electronic structure of Cd(II) multidecker phthalocyanine compounds, where the authors take into account the spin-orbit interaction. Other authors show interest in molecular structure, vibrational spectra and electronic spectra of complexes like Oxo-Titanium (oxo-Ti) porphyrin, octamethylporphyrin, Pz, and Pc complexes [21, 22]. Muranaka et al. [23] reported the synthesis of a family of Pz and Pc with Ti(IV) as central metal. They found that the monomeric complexes [TiO-Pz-*t*Bu] show interesting properties like fluorescent emission and that this luminescence is quenched when the cyclic trimer with triangular prismatic structure is formed, and this trimer is obtained by a reaction between the monomer [TiO-Pz-*t*Bu] and 2,3,6,7,10,11-hexahydroxytriphenylene, and also, they synthesized the monomer [Ti(IV)-Pz-*t*Bu(catechol)] with axial ligand catechol. This axial ligand is widely studied and used in a variety of compounds because of their extraordinary affinity with high oxidation state metals [6, 25].

Our group has centred its attention in the theoretical study of the molecular properties of the family of Ti(IV)-Pz synthesized by Muranaka et al. [23]. In this work, we performed geometry optimization and molecular orbitals calculations employing the zeroth order regular approximation (ZORA) Hamiltonian including scalar relativistic corrections [26, 27], we also carried out the characterization of electronic transitions in the absorption spectra of complexes: **1** [TiO(Pz-tetra-*t*Bu)], **2** [Ti(Pz-tetra-*t*Bu)(catechol)], **5** [Ti_3(Pz-tetra-*t*Bu)$_3$L] with L is axial ligand **a** 2,3,6,7,10,11-hexahydroxytriphenylene, and **6** [Ti(Pc-tetra-*t*Bu)(catechol-COOH)]. Because of the quite good agreement of our results with the experimental data, we were able to propose the theoretical study of the complexes **3** [Ti(Pz-tetra-*t*Bu)L], **4** [Ti_2(Pz-tetra-*t*Bu)$_2$L], and **7** [Ti(Pz-tetra-*t*Bu)(catechol-COOH)], that are not yet reported in the literature. The Pz macrocycles in all complexes are *tetra*-substituted with *tert*-butyl group (*t*Bu). Figure 1 presents a diagram of all complexes analyzed and their respective symmetry restriction. The Ti metal was elected because of the fact that it is more interesting than other metals as the axial ligation is possible to it, being a good option to introduce a motif

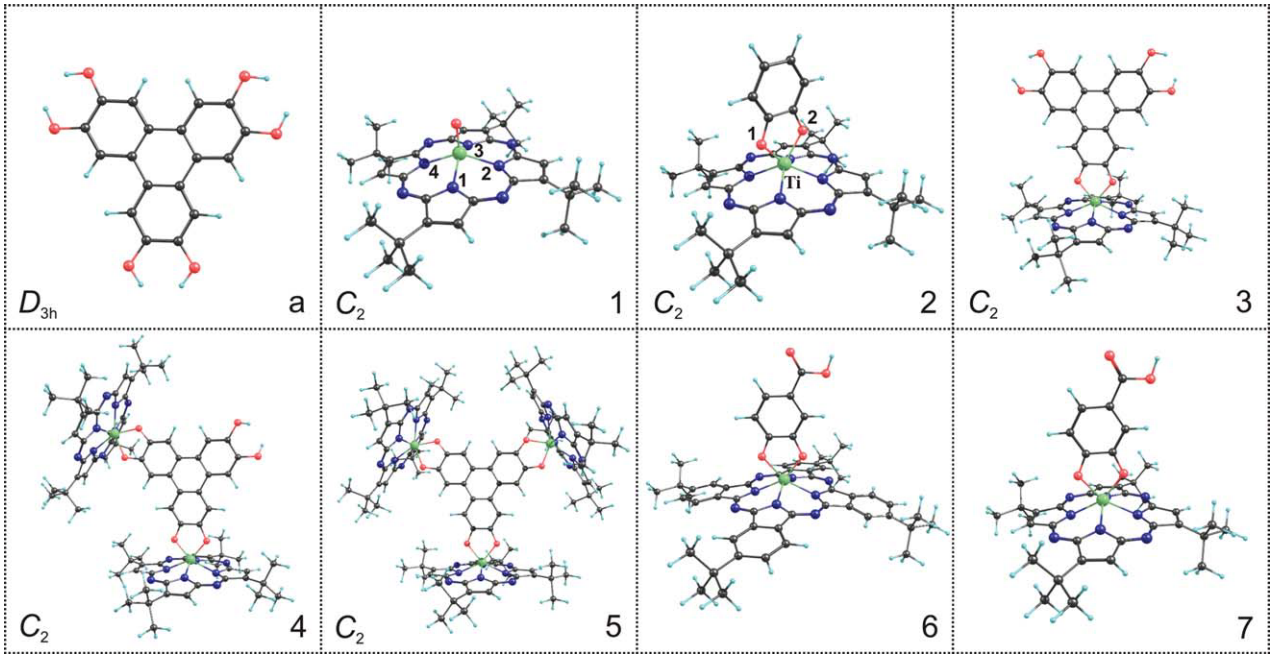

FIGURE 1. Complexes: **a**, axial ligand: 2,3,6,7,10,11-hexahydroxytriphenylene; **1**, Monomer [TiO(Pz-tetra-*t*Bu)]; **2**, Monomer with axial ligand catechol [Ti(Pz-tetra-*t*Bu)(catechol)]; **3**, [Ti(Pz-tetra-*t*Bu)L]; **4**, [Ti_2(Pz-tetra-*t*Bu)$_2$L]; **5**, [Ti_3(Pz-tetra-*t*Bu)$_3$L] with L = **a**; **6**, [Ti(Pc-tetra-*t*Bu)(catechol-COOH)]; and **7**, [Ti(Pz-tetra-*t*Bu)(catechol-COOH)]. In the complexes labeled **1** and **2**, it is possible to find the numeration used for the description of geometrical parameters. [Color figure can be viewed in the online issue, which is available at wileyonlinelibrary.com.]

with an appropriate anchor group to fasten the dye to the semiconductor nano-particles [19, 23, 28]. Complex **6** was synthesized and proved in DSC [6]; for this reason, our aim was to make a detailed analysis of the properties of all the systems to propose the possible application of the other complexes studied here for the design of solar cell devices. The calculations of excitations were carried out using the TDDFT method [29, 30] with the van Leeuwen–Baerends (LB94) model [31] implemented in the Amsterdam density functional package (ADF2008) computational code [32], which have been widely used in diverse theoretical studies. The performed predictions have been compared with all the available structural and spectroscopic information and new information is now provided about the coordination and electronic properties of a family of metallic Pz.

2. Theoretical Methodology

All calculations reported here were performed using DFT using the ADF 2008 [32] via the ZORA Hamiltonian including scalar relativistic corrections [26, 27], employing slater type orbitals basis sets with triple-ζ accuracy plus two polarization functions (TZ2P) for all the atoms [33, 34].

Monomer oxo-Ti conformation complex **1** was used as the starting point in the geometry optimizations resulting the monomer with catechol as axial ligand complex **2**, the monomer complex **7** with catechol-COOH as axial ligand, monomer with 2,3,6,7,10,11-hexahydroxytriphenylene as axial ligand complex **3**, also the dimer connected by largest axial ligand complex **4**, and the complex with structure constituted by three monomers connected through the largest axial ligand complex **5**, and the last one is the phthalocyanine with axial ligand catechol-COOH complex **6**. The optimization of the isolated largest axial ligand was made. The molecular geometry of the ground states was fully optimized via the analytical energy gradient method implemented by Verluis and Ziegler, using the local density approximation (LDA) within the Vosko–Wilk–Nusair parametrization for local exchange correlations [35, 36] and the most popular generalized gradient approximated potentials by Becke for exchange and Perdew et al. for correlation, BP86 functional [37, 38]. The excitation energies were estimated by TDDFT [29, 30]

based on the linear response formalism within the iterative Davison procedure as implemented in the ADF2008 code, employing the LB94 potential [31] used almost without exception in the applications of TDDFT. The calculations performed by first-principles method let us to obtain accurate excitation energies and oscillator strengths. Solvation effects for geometry optimizations and TDDFT calculations were modeled by means of continuum solvation models, using Conductor-like Screening Model [39] using toluene as solvent. For the charge distribution calculation, three algorithms were employed: classical Mulliken, Hirshfeld, and Voronoi deformation density (VDD) population analysis [40, 41].

3. Results and Discussion

3.1. GEOMETRICAL STRUCTURES

The calculated geometrical parameters, Ti-O, Ti-N distances and N-Ti-N and O-Ti-O angles are reported in Table I. It is possible to observe that the molecular structure calculated with LDA functional shows bond distances 0.03–0.05 Å shorter than those calculated using BP86 functional, as expected [42].

In general, in the cases where complexes contain an axial ligand, the Ti-N1 and Ti-N3 distances are slightly shorter than Ti-N2 and Ti-N4, so this suggests that the axial ligand affects the geometrical parameters of the Pz macrocycle [being this in complexes **2**, **6**, and **7**, the axial ligand catechol and in complexes **3**–**5** 2,3,6,7,10,11-hexahydroxytriphenylene]. About these bond distances in complex **1**, Zakharov et al. [21] carried out DFT calculations using the B3LYP hybrid functional and triple-ζ valence basis sets of [TiO-Pz] with hydrogen as peripheral substituent. They found that the Ti-O distance is 1.62 Å and Ti-N distances are 2.07 Å, values that are near to the calculated with LDA by us using -*t*Bu like peripheral substituent, 1.63 and 2.06 Å for complex **1**, respectively. In complexes studied here, the hole size of the macrocycle Pz is bigger than the hole size in MgPz, ZnPz, and NiPz, showing the Metal-N distance equal to 1.998, 1.981, and 1.894 Å, respectively [43]. The Ti-O distance in complex **1** is shorter than those Ti-O distances in the rest of the complexes which are formed by macrocycles of Pz and the different axial ligands. This increment in the bond distances may be due to steric effect generated by the large axial ligands.

TABLE I
Selected bond distances (Å) and angles (°) of the molecular structures in complexes 1–7 calculated at LDA and BP86 with TZ2P basis set theoretical level.

Geometrical parameters	1		2		3		4		5	6		7	
	LDA	BP86	LDA	BP86	LDA	BP86	LDA	BP86	LDA	LDA	BP86	LDA	BP86
d(Ti-O_1)	1.630	1.656	1.907	1.942	1.919	1.952	1.914	1.961	1.922	1.937	1.948	1.930	1.956
d(Ti-O_2)	–	–	1.907	1.942	1.919	1.952	1.929	1.938	1.922	1.959	1.971	1.946	1.981
d(Ti-N_1)	2.058	2.083	2.074	2.109	2.048	2.085	2.047	2.081	2.045	2.097	2.098	2.047	2.136
d(Ti-N_2)	2.058	2.083	2.077	2.113	2.101	2.142	2.097	2.130	2.098	2.149	2.155	2.097	2.082
d(Ti-N_3)	2.058	2.083	2.074	2.109	2.048	2.085	2.047	2.080	2.045	2.097	2.098	2.047	2.134
d(Ti-N_4)	2.058	2.083	2.077	2.113	2.101	2.142	2.102	2.140	2.098	2.147	2.155	2.097	2.081
$<$(N_1-Ti-N_3)	141.1	140.6	134.6	132.7	139.9	137.5	140.1	138.7	140.1	139.4	139.2	138.9	137.6
$<$(N_2-Ti-N_4)	141.1	140.6	133.8	132.1	129.2	126.9	129.7	127.7	129.7	130.0	129.0	128.5	127.2
$<$(O_1-Ti-O_2)	–	–	78.6	78.4	78.1	78.0	78.1	78.2	78.1	77.2	77.9	77.9	77.9

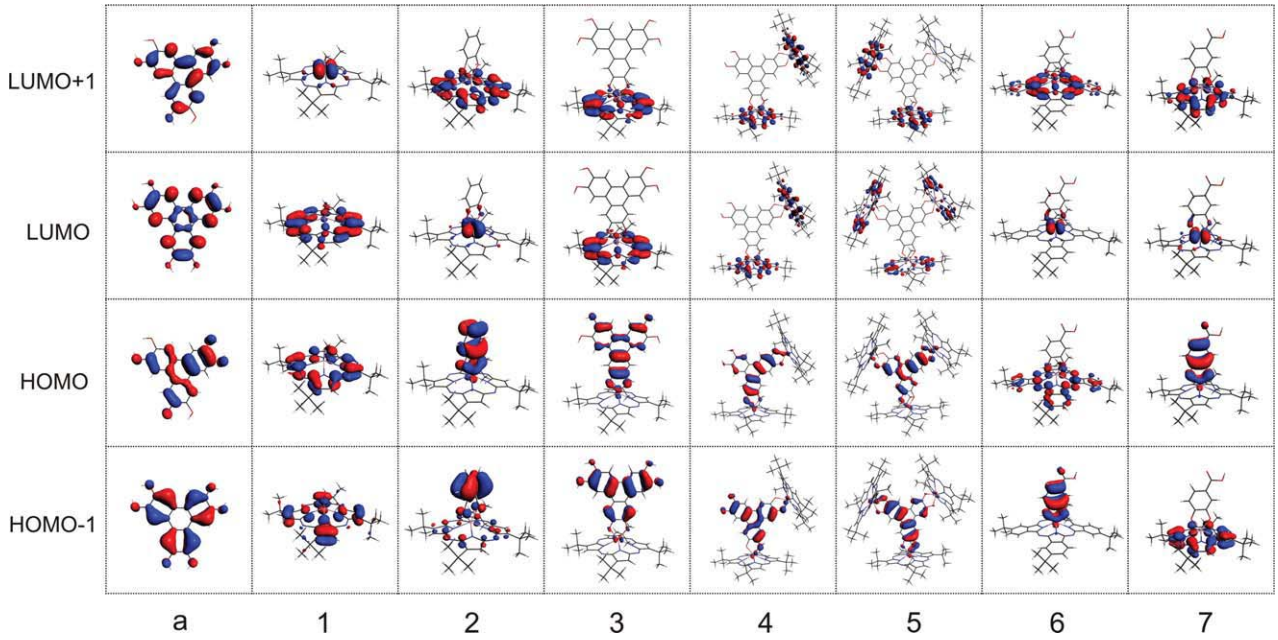

FIGURE 2. Diagrams for the calculated frontier MOs of complexes **1–7** and axial ligand **a**. [Color figure can be viewed in the online issue, which is available at wileyonlinelibrary.com.]

In the same way, in all compounds the angles formed by N_1-Ti-N_3 and N_2-Ti-N_4 calculated with LDA are larger (approxiamtely 1 or 2°) than the obtained using BP86 functional; but the angles O_1-Ti-O_2 in the complexes **2–4** are very similar with both functionals, and the complex **5** was not optimized using BP86 functional because of their large dimensions and limited computational resources.

On the other hand, it is important to pay attention on the central metal Ti(IV). Its position is out of plane of the four central nitrogen atoms of the Pz forming a square pyramid with them, (Fig. 1) due to its large atomic radii (~1.47 Å) and the short cavity diameter of Pz (approximatly around 4 Å). This aspect could influence the planar geometry of the Pz ring and when it is necessary it could mediate in the reactivity of the complexes. As can be seen in the Table I, the angle N_2-Ti-N_4 decreases with respect to angle N_1-Ti-N_3, when the ligand catechol is introduced (in complex **2**) and when two or more Pz macrocycle constitute the systems. In other words, the progressive displacement out of Pz plane is observed to be on going from complexes **1** to **7**, although the system turns more bulky.

The axial ligand **a** is the most symmetric moiety. It has four rings in the same plane and show an almost D_{3h} overall symmetry. Partly because of -*t*Bu peripheric substituents, the complexes **1**, **2**, **3**, and **4** have only two symmetric elements corresponding to identity and C_2 principal axe, which indicate that the equilibrium structures show C_2 symmetry, the trimer **5** that forms a trigonal prism presents a D_3 symmetry, and finally the complexes **6** and **7** do not show any symmetry.

3.2. MOLECULAR ORBITAL AND ENERGY LEVELS

The isosurface plots of the frontier molecular orbitals are depicted in Figure 2, and the diagram of the ground state levels of complexes **1–7** are shown in Figure 3.

In Figure 2, we can see that occupied orbitals of the isolated ligand **a** are formed by "*p*" antibonding orbitals localized on the C and O atoms; these orbitals form a π-cloud of antibonding character. In complex **1**, the frontier MOs are localized in the macrocycle Pz without a meaningful contribution of the -*t*Bu groups, but the LUMO+1 are constituted by unoccupied "*d*" orbitals of the Ti(IV) metal, specifically $d_{x^2-y^2}$ and d_{xy} orbitals.

In complex **2**, the occupied frontier molecular orbitals are centred on the catechol axial ligand. In the LUMO take part, the d_{z^2} and d_{xy} orbitals of the metal and the LUMO+1 is localized on the Pz ring. This fact indicates that electronic transitions with

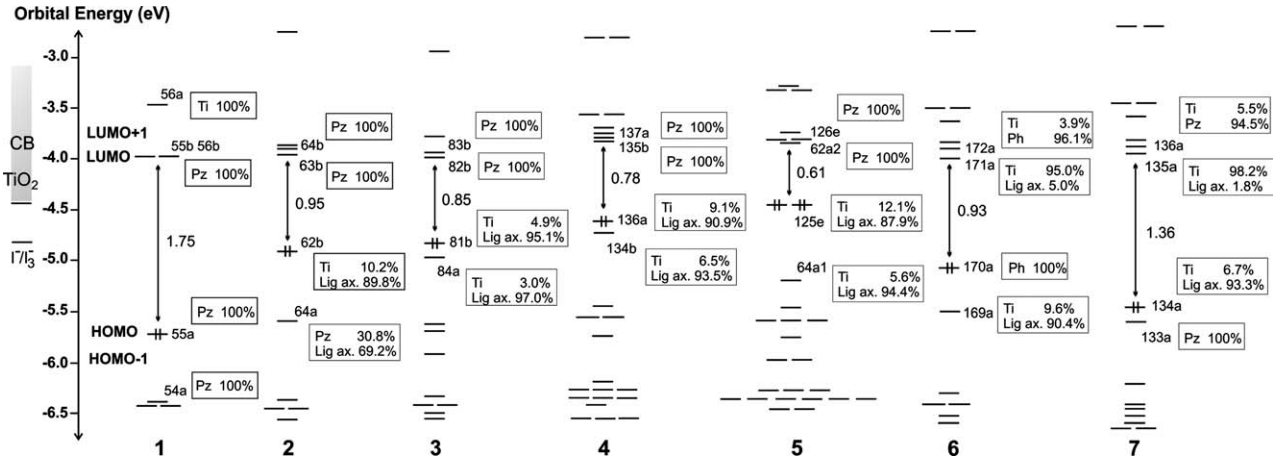

FIGURE 3. Orbital energy levels and decomposition of frontier MOs in complexes **1**–**7**.

low energy, may involve an important charge transfer directed to the Pz or toward the Ti(IV) atom.

On the other hand, the energies of the HOMO and HOMO−1 are near in complexes **3**, **4**, and **7** but not in complexes **1**, **2**, **5**, and **6**. The LUMO and LUMO+1 in all cases are almost degenerated except in complex **1** (Fig. 3). In complexes **3**, **4**, and **5**, these orbitals are constituted by "*p*" orbitals localized in the Pz ring, and in the complexes that contain catechol, the LUMO is centered in the metal center and the LUMO+1 in the macrocycle. These results indicate that the inclusion of the COOH substituent in the catechol and the change of the macrocycle from porphyrazine in complex **7** to phthalocyanine in complex **6** do not change the contribution orbital to the frontier unoccupied molecular orbitals.

On the other hand, the HOMO in complex **6** and the HOMO−1 in complex **7** are constituted by "*p*" orbitals in the macrocycle; the HOMO−1 in complex **6** and the HOMO in the complex **7** are constituted by an antibonding combination of "*p*" orbitals localized in the catechol ligand. On the contrary to these results, the calculations performed with semiempirical method for the complex **6**, indicated that the LUMO orbital is localized over the macrocycle [6], with minimal participation from the Ti metal.

On the other hand, the complex **6** has been proven in solar cells showing efficient electronic injection to semiconductor nanoparticles. Taking this into account, the similar electronic properties of complex **6** and complexes **2**, **3**, **4**, and **7**, it is possible to say these complexes could act as good sensitizers in a solar cell device showing electronic injection to the semiconductor and then create a circuit current [16]. This is supported on that the LUMO in all the described complexes including the complex **6** has higher energy value than the position of the lower level of the TiO_2 conduction band or conduction band edge (Fig. 3), because if the LUMO energy is below the TiO_2 conduction band edge, it possibly predict an unfavorable electron injection originating from the sensitizer [44–48]. The complexes **2**, **3**, and **7** show a HOMO energy very near to HOMO energy of redox couple I^-/I_3^- (being this couple used in the regeration of the dye in a DSC [9–11]), together with the fact that the complexes show an important absorption in the visible region (vide infra). Besides, it could be important for the charge separation, which may facilitate the electron injection from the dye to the conduction band of semiconductor, and this can be analyzed through the compositons of the HOMO and LUMO, where the HOMO is localized in the donor motif and the LUMO over the acceptor subunit [49–51].

On the other hand, complexes **3**, **4**, and **7** could anchor to TiO_2 nanoparticles through the carboxylic acid or hydroxyl groups in the axial ligands, which including phosphate are generally used to link the dye to the surface of the TiO_2 nanoparticles [52]. Otherwise, complex **5** could not be used in this type of devices because it has the shortest HOMO–LUMO gap than all remaining complexes and it is feasible to go through a vibrational dacayment way. These results also give us an explanation about the fact, that the trimer complex **5** does not shown any luminescent properties, which disappear on trimerization.

TABLE II

Charge transfer (CT) calculated for Ti atoms and their orbital occupation obtained with Mulliken analysis.

Complexes	Mulliken	Orbital occupation	Hirshfeld	Voronoi
1	2.47	$s^{0.04}\ p^{0.14}\ d^{2.24}\ f^{0.05}$	3.55	3.63
2	2.61	$s^{0.05}\ p^{0.28}\ d^{2.22}\ f^{0.06}$	3.52	3.62
3	2.65	$s^{0.05}\ p^{0.31}\ d^{2.23}\ f^{0.05}$	3.54	3.64
4[a]	2.65	$s^{0.05}\ p^{0.31}\ d^{2.23}\ f^{0.05}$	3.55	3.64
5[b]	2.76	$s^{0.07}\ p^{0.28}\ d^{2.35}\ f^{0.06}$	3.57	3.66
6	2.51	$s^{0.01}\ p^{0.27}\ d^{2.23}\ f^{0.00}$	3.53	3.63
7	2.51	$s^{0.01}\ p^{0.26}\ d^{2.24}\ f^{0.00}$	3.54	3.63

[a] The same data is for the two Ti atoms in the complex.
[b] The same data is for the three Ti atoms in the complex.

We performed the charge transfer analysis of the Ti(IV) in all complexes, which was calculated from the difference between the expected charge of the metal in the complexes and the charge of the metal obtained by the calculations employing the Mulliken, Hirshfeld, and Voronoi models. Here, the metal has d^0 electronic configuration. In this analysis (Table II), Hirshfeld and Voronoi models show a meaningful electron donation that occurs from the ligand to the metallic center. The charge transfer from Pz to metal center in the ground state obtained by Mulliken population analysis reproduces the smallest values and shows a behavior of less covalent character than the obtained with Hirsfeld and Voronoi models; thus, these last models reproduce the chemical behavior of the systems in a better way, because the macrocycle Pz is predominantly π donor ligand and therefore it favored the charge transfer to the empty orbitals of the Ti(IV) atom. These three analyses show that the charge transfer is indicative of the interaction between the ligand and metallic atom and that has some covalent character, for that reason it is feasible to consider that the coordination energy will be influenced by this charge transfer. Additionally, the occupation of the valence shell in Ti(IV) centers are included in Table II. The electronic configuration of Ti(IV) is $[Ne]3s^2\ 3p^6\ 3d^0\ 4s^0$, and the configurations calculated by Mulliken analysis in the complexes show that the charge transfered to metal is distributed between the empty orbitals. In consequence, the metal could act as an electronic charge carrier or electronic charge receptor.

3.3. TDDFT ANALYSIS: ABSORPTION SPECTRA

Before the peaks assignment of the simulated spectra, it is useful to have a general view of the solution absorption spectra of metallic Pz. The UV–vis absorption spectra are characterized by a weak *Q* band that is usually responsible for the strong absorption in the visible region showing two peaks ~600 nm and 550 nm, other characteristic band is observed in the near UV corresponding to the *B* band or "Soret" band [43]. The highest occupied orbitals HOMO and HOMO−1 and the lowest unoccupied orbitals LUMO and LUMO+1 are some of the orbitals involved in these transitions, which are the four orbitals whose significance for the UV–vis absorption spectra has been studied by Gouterman [53].

The excitation energies and oscillator strengths calculated for the absorption spectra of the complexes **1**–**7** are reported in Table III and compared with the experimental data. The surface of each peak must be proportional to oscillator strength (*f*) and this latter also give information about the probability that the transition occurs. Here, the calculated *f* on isolated molecules provides the same qualitative trend that the intensities of the *Q* bands present in the visible region of the spectra (Fig. 4) [21]. The most intense bands are present in the spectra of the prism **5** and the phthalocyanine **6** followed by the monomer **1** and then the less intense correspond for complex **2**. The other systems studied complexes **3**, **4**, and **7** show that the *Q* and *B* bands in these complexes have bigger oscillator strength values than the bands in the complex **1** and **2** and shorter than in the bands in the spectra of complex **5**.

In complex **1**, we assigned both *Q* and *B* bands as being the ligand-centred $\pi \rightarrow \pi^*$ transitions ligand to ligand charge transfer (LLCT) type. The *Q* band is observed at 575 nm and involves a transition 55a → 55b from the HOMO to LUMO+1 with contribution of 75.5%, those two orbitals are localized in the macrocycle Pz. In the *B* band, the contribution of the 45a → 55b

TABLE III

Experimental and calculated wavelength (nm), energy (eV), oscillator strength *f* (×100), active MOs and their contributions, and type of the electronic transitions for the vertical excitations from TDDFT.

Complexes	Assignment	λ (nm) Experimental	λ (nm) Calculated	E (eV)		*f* (×100)	Active MOs	Contribution (%)	Transition type
1	*Q*	600	575	2.16	2.43[a]	10.35	55a → 55b	75.5	LLCT
							51a → 56b	11.1	LLCT
		550	545	2.27		0.11	54a → 55b	96.1	LLCT
	B	350	325	3.82		3.68	45a → 55b	63.1	LLCT
							48a → 56b	14.4	LLCT
2	*Q*	600	579	2.14		1.90	62a → 65a	76.3	LMCT
							61a → 65a	17.8	LMCT
		550	555	2.24		0.06	60a → 65a	95.1	LMCT
	B	350	353	3.52		0.04	63a → 68a	90.3	L-LMCT
3	*Q*		574	2.16		16.20	81b → 84b	60.9	LMCT
							80a → 85a	15.1	LMCT
			540	2.30		0.41	80a → 85a	54.8	LMCT
							81a → 85a	27.2	LMCT
	B		343	3.62		11.94	76b → 84b	82.2	LMCT
4	*Q*		594	2.09		12.73	133b → 139a	24.3	LLCT
							134a → 137b	20.2	LLCT
							133b → 138a	10.2	LLCT
			561	2.21		2.96	133a → 137a	62.4	LMCT
							130b → 135b	18.6	LMCT
	B		348	3.56		1.99	118b → 135b	80.9	LMCT
5	*Q*	600	593	2.09		19.96	63a1 → 63a2	23.2	LLCT
							124e → 127e	46.1	LLCT
							123e → 127e	11.1	LLCT
		550	555	2.24		9.37	125e → 67a1	21.3	LLCT
							123e → 126e	26.1	LLCT
							123e → 62a2	12.1	LLCT
	B	350	363	3.42		2.23	56a2 → 65a1	91.2	LMCT
6	*Q*	702	724	1.71		22.41	170a → 173a	84.9	LLCT
		640	656	1.89		10.94	170a → 175a	78.8	L-MLCT
							170a → 172a	13.4	LLCT
		350	364	3.41		18.52	156a → 173a	17.4	LLCT
							158a → 173a	14.4	LLCT
							150a → 173a	14.2	LLCT
	B	300	324	3.82		10.25	155a → 175a	45.7	L-MLCT
							140a → 172a	14.0	LLCT
							143a → 173a	7.6	LLCT
7	*Q*		610	2.03		5.22	133a → 136a	65.2	LLCT
							132a → 136a	9.0	LLCT
			555	2.24		3.22	127a → 135a	32.1	LMCT
							132a → 137a	15.4	LLCT
	B		362	3.42		13.69	124a → 138a	35.5	L-MLCT
							134a → 141a	20.4	LLCT
							120a → 137a	15.5	LLCT

[a] Energy value reported for the absorption specter of the monomer at B3LYP theoretical level [TiO-Pz] [21].

configuration mixes with other configuration (48a → 56b), which is of LLCT nature.

Our calculations for the monomer **1** with -*t*Bu substituents compared with calculations performed on the octamethyl substituted [TiO-Pz] [20] indeed show that the -*t*Bu substituents have effect over the *Q* band energy (Table III). There is an agreement quite close with Sundholm [54], who

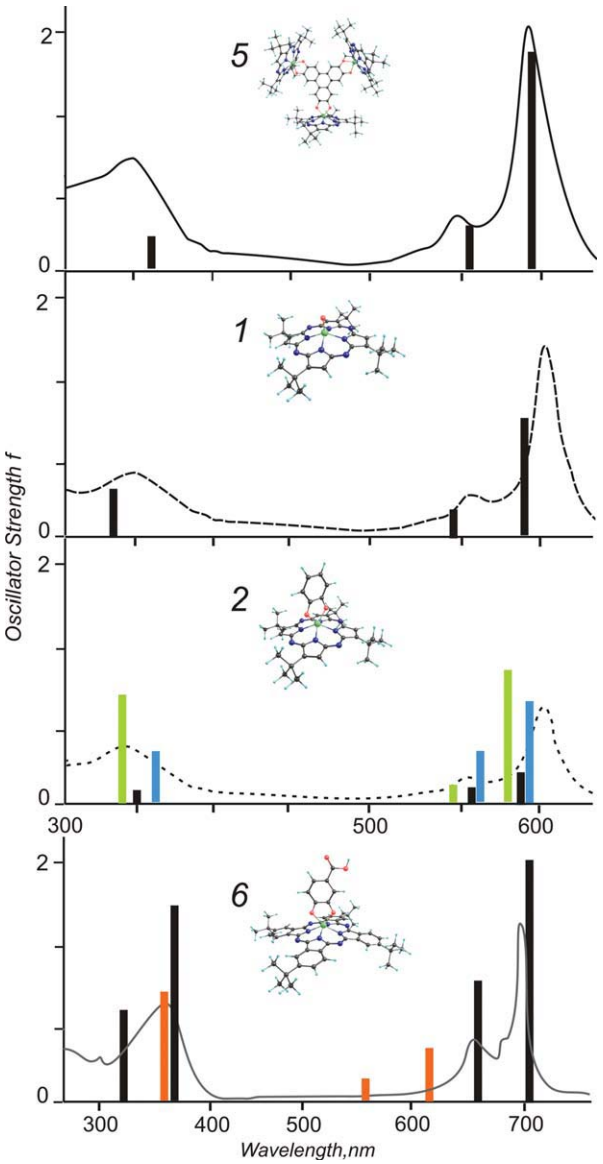

FIGURE 4. Diagrams for the experimental absorption spectra of complexs **5**, **1**, **2** and **6** with continuous line, also thick black bars show the peaks calculated for the complexes reported. The gray bars show the peaks calculated for complex **3**, gray dashed bars for complex **4**, and dark gray ones for complex **7**. [Color figure can be viewed in the online issue, which is available at wileyonlinelibrary.com.]

has also investigated the influence of the alkyl substitution in porphyrins, stating that the substitutions may produce excitation energies downward shifts of as much as 0.2–0.3 eV.

From the other side, ligand to metal charge transfer (LMCT) transitions are also expected to play a role in complexes **2**–**7** because of the presence of d_{xy} orbitals into the valence region. In complex **2**, the *Q* band is characterized by a LMCT transition which is mainly (76%) described by the (62a → 65b) (HOMO−3 → LUMO) excitation, and the (61a → 65b) (HOMO−4 → LUMO) transition with only a weight of 18%. According to these results, the (63a → 68a) state calculated at 3.52 eV (353 nm) in complex **2** are responsible for the *B* band appearing in the spectrum and it is from catechol ligand to metallic orbitals with some contribution of the catechol. The complex **7** that is constituted by Pz with ligand catechol-COOH show three absorption bands, which show a red shift less than 12 nm with respect to the bands in complex **2**. In complex **3**, the *Q* band is assigned to (81b → 84b) excitation and it mixes with the (80a → 85a) state, and this last undergoes configuration interaction with the nearly degenerate (80a → 85a) and (81a → 85a) states of the band centred at 540 nm. The *Q* and *B* bands are assigned as LMCT type. The latter shows that in complexes **2** and **3** the transitions are largely directed toward the metal in the Pz.

In the complex **4** with two macrocycles, the weak excited state at 2.09 eV, which is mainly described by a $\pi \rightarrow \pi^*$ transition of LLCT type, show a mixture of the (133b → 139a), (134a → 137b), and (133b → 138a) states. Specifically for complex **5**, the weaker excitation are underestimated by around 7 nm and is constituted by the transitions namely ($63a_1 \rightarrow 63a_2$), (124e → 127e), and (123e → 127e) which are mixed. This explains why the contribution percents are low in the three transitions; in the same way it occurs with the configuration corresponding to the higher energy *B* band.

The complex **6** shows four bands in the experimental absorption spectra, 702, 640, 350, and 300 nm, and the calculated wavelengh show only a red shift around 20 nm. The *Q* band suffers a split in the two more intense bands in the visible region. The *Q* band with minor energy corresponding to $\pi \rightarrow \pi^*$ transition being of the LLCT type, and the *Q* band found at 656 nm has metal contribution in the excited state.

The TDDFT/LB94 model appears to obtain lower excitation energies for the *B* bands in complex **5** when compared with experimental description, although the *Q* bands are better described. The differences do not lead to major discrepancies in the assignments of the electronic transitions of the experimental bands.

4. Conclusions

The study of the molecular properties have been performed via relativistic scalar ZORA Hamiltonian,

where the results indicate a good description of the electronic structure, which is also proved with the quite good agreement observed between the experimental data and the absorption spectra of series of Ti(IV)-Pz. Specifically as can be noticed in Table III, the visible region is dominated by *Q* bands centred at 575 nm in complex **1**, 579 nm in complex **2**, 564 nm in complex **3**, 594 nm in complex **4**, and 593 nm in complex **5**, 724 and 656 nm in complex **6**, and 610 nm in complex **7**, respectively, and the *B* bands are near to UV region ~350 nm in all the analyzed complexes.

The calculated properties in complexes **2**, **3**, **4**, and **7**, like high absorption in the visible region of the spectra, and the transitions involved in these bands with a determined direction, from the occupied orbitals of the axial ligands (catechol in complexes **2** and **7** and **a** in complexes **3** and **4**) to unoccupied orbitals localized in the metal center or Pz ring, indicate that this direction of the transitions could create a charge separation and simplify the electronic injection to the semiconductor, besides they have a natural role in light harvesting mainly in the range of 400–700 nm. These complexes present bigger HOMO–LUMO gap than the complex **5**, and the energy of their LUMO orbitals are bigger than the lowest energy level of the TiO_2 conduction band. Then, with these results in mind, we consider that complexes **2**, **3**, **4**, and **7** are appropriate for their potential use in solar cells devices.

For complex **1**, the peripheral substitution with -*t*Bu change slightly the geometrical parameters in the Pz ring, the differences of the Ti-O and Ti-N distances in the complex without alkyl substituent [21] with **1** is 0.01 Å. In others systems, these distances change because of the inclusion of the axial ligands. The results of Hirsfeld and Voronoi charge transfer analysis proved that they are numerically very similar and yield chemically meaningful charge transfers, which indicate that the interaction metal-ligand has more covalent than electrostatic character.

References

1. Wei-Jun, Y.; Can-Cheng, G.; Zi-Yang, L.; Neng-Ye, T. J Porphyrins Phthalocyanines 2009, 13, 973.
2. Gregory, P. J Porphyrins Phthalocyanines 2000, 4, 432.
3. Leng, F.; Hou, R.; Jin, L.; Yin, B.; Xiong, R. G. J Porphyrins Phthalocyanines 2010, 14, 108.
4. Campbell, W. M.; Jolley, K. W.; Wagner, P.; Wagner, K.; Walsh, P. J.; Gordon, K. C.; Schmidt-Mende, L.; Nazeeruddin, M. K.; Wang, Q.; Grätzel, M.; Officer, D. L. J Phys Chem C 2007, 111, 11760.
5. Campbell, W. M.; Burrell, A. K.; Officer, D. L.; Jolley, K. W. Coord Chem Rev 2004, 248, 1363.
6. Palomares, E.; Martínez-Díaz, M. V.; Haque, S. A.; Torres, T.; Durrant, J. R. Chem Commun 2004, 2112.
7. Imahori, H.; Umeyama, T.; Ito, S. Acc Chem Res 2009, 42, 1809.
8. Grätzel, M. Acc Chem Res 2009, 42, 1788.
9. Xie, Y.; Joshi, P.; Ropp. M.; Galipeau, D.; Zhang, L.; Fong, H.; You, Y.; Qiao, Q. J Porphyrins Phthalocyanines 2009, 13, 903.
10. Varotto, A.; Chang-Yong, N.; Radivojevic, I.; Tomé, J. P. C.; Cavaleiro, J. A. S.; Black, C. T.; Drain, C. M. J Am Chem Soc 2010, 132, 2552.
11. Grätzel, M. Inorg Chem 2005, 44, 6841.
12. Thompson, B. C.; Fréchet, J. M. J. Angew Chem 2008, 47, 58.
13. Nazeeruddin, M. K.; De Angelis, F.; Fantacci, S.; Selloni, A.; Viscardi, G.; Liska, P.; Ito, S.; Takeru, B.; Grätzel, M. J Am Chem Soc 2005, 127, 16835.
14. Gao, F.; Wang, Y.; Shi, D.; Zhang, J.; Wang, M.; Jing, X.; Humphry-Baker, R.; Wang, P.; Zakeeruddin, S. M.; Grätzel, M. J Am Chem Soc 2008, 130, 10720.
15. Yum, J. H.; Chen, P.; Grätzel, M.; Nazeeruddin, M. K. Chem Sus Chem 2008, 1, 699.
16. Fitzgerald, J.; Taylor, W.; Owen, H. Synthesis 1991, 686.
17. Rodríguez-Morgade, M. S.; Stuzhin, P. A. J Porphyrins Phthalocyanines 2004, 8, 1129.
18. Mozer, A. J.; Griffith, M. J.; Tsekouras, G.; Wagner, P.; Wallace, G. G.; Mori, S.; Sunahara, K.; Miyashita, M.; Earles, J. C.; Gordon, K. C.; Du, L.; Katoh, R.; Furube, A.; Officer, D. L. J Am Chem Soc 2009, 43, 15621.
19. Morokuma, N.; Kobayashi, N. Coord Chem Rev 2002, 227, 129.
20. Baumann, T. F.; Barrett, A. G. M.; Hoffman, B. M. Inorg Chem 1997, 36, 5661.
21. Zakharov, A. V.; Girichev, G. B. J Mol Struct Theochem 2008, 851, 183.
22. Muranaka, A.; Okuda, M.; Kobayashi, N.; Somers, K.; Ceulemans, A. J Am Chem Soc 2004, 126, 4596.
23. Muranaka, A.; Yoshida, K.; Akagi, Y.; Naka, H.; Uchiyama, M.; Kondo, Y.; Kobayashi, N. Tetrahedron Lett 2008, 49, 5084.
24. Muñoz-Castro, A.; Mac-Leod Carey, D.; Arratia-Pérez, R. Polyhedron 2010, 29, 451.
25. Kojima, T.; Hirasa, N.; Noguchi, D.; Ishizuka, T.; Miyazaki, S.; Shiota, Y.; Yoshizawa, K.; Fukuzumi, S. Inorg Chem 2010, 49, 3737.
26. van Lenthe, E.; Baerends, E. J.; Snijders, J. G. J Chem Phys 1994, 101, 9783.
27. Velde, G. T.; Bickelhaupt, F. M.; van Gisberger, S.; Fonseca-Guerra, C.; Baerends, E. J.; Snijders, J. G.; Ziegler, T. J Comput Chem 2001, 22, 931.
28. Yu, C.; Hanack, M.; Werner, J. B.; Danilo, D.; Ying, L.; Ying, L.; Jinrui, B. J Mater Sci 2006, 41, 2169.
29. Runge, E.; Gross, E. K. U. Phys Rev Lett 1984, 52, 997.
30. Wang, F.; Ziegler, T.; van Lenthe, E.; van Gisbergen, S. Baerends, E. J. J Chem Phys 2005, 122, 204103.

31. van Leeuwen, R.; Baerends, E. J Phys Rev A 1994, 49, 2421.
32. Amsterdam Density Functional (ADF) Code, Release 2009; Vrije Universiteit: Amsterdam, The Netherlands, 2009.
33. Snijder, J. G.; Baerends, E. J.; Vernooijs, P. At Nucl Data Table 1982, 26, 483.
34. Vernooijs, P.; Snijders, J. G.; Baerends, E. J. Slater Type Basis Functions for the Whole Periodic System. Internal Report; Free University of Amsterdam: The Netherlands, 1981.
35. Verluis, L.; Ziegler, T. J Chem Phys 1988, 88, 322.
36. Vosko, S. H.; Wilk, L.; Nusair, M. Can J Phys 1980, 58, 1200.
37. Perdew, J. P.; Chevary, J. A.; Vosko, S. H.; Jackson, K. A.; Pederson, M. R.; Singh, D. J.; Fiolhais, C. Phys Rev B 1992, 46, 6671.
38. Perdew, J. P.; Yue, W. Phys Rev B 1986, 33, 8800.
39. Klamt, A.; Jonas, V. J Chem Phys 1996, 105, 9972.
40. Guerra, C. F.; Handgraaf, J. W.; Baerends, E. J.; Bickelhaup, F. M. J Comput Chem 2004, 25, 189.
41. Nalewajski, R. F. Phys Chem Chem Phys 2002, 4, 1710.
42. Koch, W.; Holthausen, M. C. A Chemist's Guide to Density Functional Theory, 2nd ed.; Wiley-VCH: Germany, 2001, p 128.
43. Baerends, E. J.; Ricciardi, G.; Rosa, A.; van Gisbergen, S. J. Coord Chem Rev 2002, 230, 5.
44. Kusama, H.; Orita, H.; Sugihara, H. Langmuir 2008, 24, 4411.
45. Kusama, H.; Sugihara, H.; Sayama, K. J Phys Chem C 2009, 113, 20764.
46. Lin, C.; Yu-Chien, W.; Hsu, S.; Lo, C.; Wei-Guang, E. J Phys Chem C, 2010, 114, 687.
47. Xiang, H.; Wei, S.; Gong, X. J Phys Chem C 2009, 113, 18968.
48. Balanay, M. P.; Hee Kim, D. Phys Chem Chem Phys 2008, 10, 5121.
49. Tachinaba, Y.; Haque, S. A.; Mercer, I. P.; Durrant, J. R.; Klug, D. R., J Phys Chem B, 2000, 104, 1198.
50. Neil, R. Angew Chem Int Ed 2006, 45, 2338.
51. Bomben, P. G.; Koivisto, B. D.; Berlinguette, C. P. Inorg Chem 2010, 49, 4960.
52. Grätzel, M. C R Chim 2006, 9, 578.
53. Gouterman, M. J Chem Phys 1959, 30, 1139.
54. Sundholm, D. Chem Phys Lett 2000, 317, 392.